

## Electrically Detected Electron-Spin-Echo Envelope Modulation: A Highly Sensitive Technique for Resolving Complex Interface Structures

Felix Hoehne,\* Jinming Lu, Andre R. Stegner, Martin Stutzmann, and Martin S. Brandt  
Walter Schottky Institut, Technische Universität München, Am Coulombwall 4, 85748 Garching, Germany

Martin Rohrmüller, Wolf Gero Schmidt, and Uwe Gerstmann  
Lehrstuhl für Theoretische Physik, Universität Paderborn, Warburger Straße 100, 33098 Paderborn, Germany  
(Received 11 March 2011; published 11 May 2011)

We show that the electrical detection of electron-spin-echo envelope modulation (ESEEM) is a highly sensitive tool to study interfaces. Taking the Si/SiO<sub>2</sub> interface defects in phosphorus-doped crystalline silicon as an example, we find that the main features of the observed echo modulation pattern allow us to develop a microscopic model for the dangling-bond-like  $P_{b0}$  center by comparison with the results of *ab initio* calculations. The ESEEM spectrum is found to be far more sensitive to the defect characteristics than the spectrally resolved hyperfine splitting itself.

DOI: 10.1103/PhysRevLett.106.196101

PACS numbers: 68.35.Dv, 61.72.Bb, 61.72.Hh, 71.55.Cn

The Si/SiO<sub>2</sub> interface is arguably the most important interface in semiconductor technology, strongly influencing device performance. Its electronic structure is decisively determined by dangling-bond-like defects, the so-called  $P_b$  centers, whose structure has been studied for decades [1]. However, detailed information cannot easily be obtained: e.g., electron diffraction techniques fail if no translational symmetry is present. At the (100)-oriented Si/SiO<sub>2</sub> interface, two kinds of paramagnetic defects, labeled  $P_{b0}$  and  $P_{b1}$ , have been studied frequently by electron spin resonance (ESR) [2–6]. Despite their omnipresence, their detailed microscopic structure is still unknown [7]. Theoretical models have so far been compared with experimental values of the two strongest hyperfine (hf) interactions as determined by continuous wave (cw) ESR [3–9]. However, for a detailed understanding of the defect structure, the weaker interactions with more distant nuclei, the superhyperfine interactions (shf), can be useful since they are very sensitive to details of the local structure. Electron-spin-echo envelope modulation (ESEEM) spectroscopy is widely used to determine weak ( $\leq 5$  MHz) hf interactions [10]. In this work, we combine the benefits of ESEEM with the enhanced sensitivity of electrically detected magnetic resonance (EDMR) when compared to conventional ESR [11]: Electrically detected ESEEM (EDESEEM) allows us to study shf interactions of the  $P_{b0}$  defect in *c*-Si:P with <sup>29</sup>Si nuclei at 4th and 5th nearest neighbor lattice sites. Comparing these values with *ab initio* calculations of the shf parameters for different structures of the  $P_{b0}$  center, we demonstrate that shf interactions with distant nuclei are an exceptionally sensitive probe for the investigation of the interface structure.

The samples used in this work were grown by chemical vapor deposition and consist of a 22 nm thick Si layer with a P concentration of  $\approx 1.0 \times 10^{17}$  cm<sup>-3</sup> on a 2.5  $\mu$ m thick, undoped Si buffer grown on a (100)-oriented

silicon-on-insulator substrate off-cut by  $\approx 1^\circ$  as determined by x-ray diffraction. The doped epilayer leads to strong <sup>31</sup>P- $P_b$  recombination, so that dominantly  $P_b$  defects at the top surface are probed [12]. In the following, we describe measurements on three samples with 4.7% (natural), 20(4)% and >98% fractions of <sup>29</sup>Si nuclei in the doped epilayer and in the top 100 nm of the buffer. For electrical measurements, interdigit Cr/Au contacts with a period of 20  $\mu$ m covering an active area of  $2 \times 2.25$  mm<sup>2</sup> have been evaporated. All experiments are performed at 5 K under illumination with above-bandgap light in a dielectric microwave resonator for pulsed EPR at X-band frequencies. The 4.7% and 20% (100%) sample are biased with 100 mV (1000 mV) to obtain the best signal-to-noise ratios. To compare different nominal surface terminations, we show the results for the Si surfaces with a native oxide (4.7% and 20% samples) as well as after exposure to 10% HF in H<sub>2</sub>O (100% sample).

In a first step, the major paramagnetic states are identified in cw EDMR experiments using magnetic field modulation (Fig. 1). Prominent signatures in all spectra result from spin-dependent recombination via <sup>31</sup>P- $P_{b0}$  spin pairs at the Si/SiO<sub>2</sub> interface [12]. In the spectrum of the <sup>nat</sup>Si (4.7% <sup>29</sup>Si) sample (black line) the two hf-split <sup>31</sup>P donor resonances inhomogeneously broadened by unresolved shf interactions with <sup>29</sup>Si nuclei (peak-to-peak linewidth  $\Delta B_{pp} = 0.37$  mT) [13] and the  $P_{b0}$  resonance ( $\Delta B_{pp} = 0.6$  mT) are visible. In the 20% <sup>29</sup>Si sample, two additional satellite lines are clearly resolved with splittings of 10.5 and 15.7 mT. The spectral positions of the inner hf-split lines can be described—referring to the [111] direction—with  $g_{||} = 2.0017(3)$  and  $g_{\perp} = 2.0088(3)$  and with a hf splitting of  $A_{||} = 14.5$  mT and  $A_{\perp} = 8.1$  mT, in good agreement with the values reported for the  $P_{b0}$  center [6]. The hf splitting of 15.7 mT and the  $g$  factor of 2.0046(8) estimated from the outer pair of peaks agree well with the

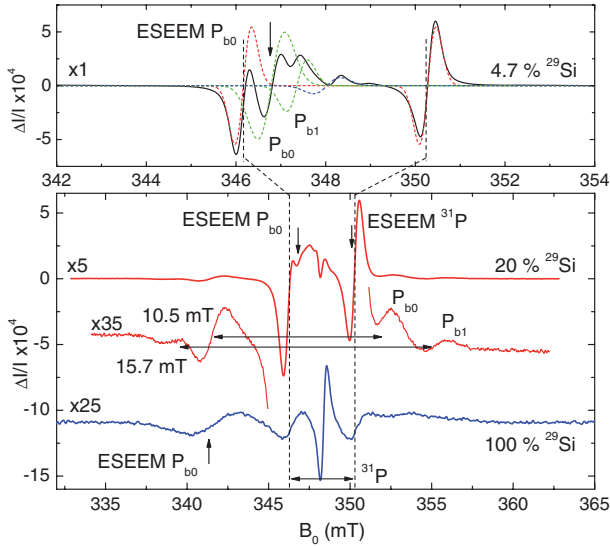


FIG. 1 (color online). Continuous wave (cw) EDMR spectra of the *c*-Si:P samples with  $^{29}\text{Si}$  fractions of 4.7%, 20% and 100% for  $\vec{B}_0 \parallel [100]$ . The upper panel shows a fitted decomposition of the 4.7% spectrum (dashed lines). For the 20%  $^{29}\text{Si}$  sample two pairs of hf-split peaks (horizontal arrows) are attributed to  $P_{b0}$  and  $P_{b1}$  spins. Vertical arrows indicate the spectral positions where ESEEM experiments have been performed.

values reported for the  $P_{b1}$  center for  $B_0 \parallel [100]$  [6]. Whereas in the 100%  $^{29}\text{Si}$  sample these lines cannot be separated due to their large inhomogeneous broadening, this assignment is supported by a weak resonance at  $g = 2.0034(5)$  ( $\Delta B_{pp} = 0.47$  mT) in the 4.7%  $^{29}\text{Si}$  sample. While there is no consensus in the literature whether the  $P_{b1}$  defect is electrically active [14,15], Fig. 1 indicates that it is in our samples. Double integration of the hf-split lines (20%) and the central  $P_b$  resonances (4.7%) suggests that the concentration of  $P_{b1}$  centers is  $\approx 1/4$  of that of the  $P_{b0}$  centers. The central line at  $g = 1.999$ , showing within a factor of 2 the same  $\Delta I/I$  for the three samples, is tentatively attributed to conduction band electrons [16].

We measured electrically detected ESEEM using a  $\pi/2$ - $\tau_1$ - $\pi$ - $\tau_2$ - $\pi/2$  spin-echo sequence, where  $\pi/2$  and  $\pi$  denote microwave pulses with corresponding flipping angles and  $\tau_1$ ,  $\tau_2$  denote the duration of periods of free evolution. This pulse sequence, thus, consists of a conventional two-pulse ESEEM experiment followed by a  $\pi/2$  projection pulse for the electrical readout of the spin [17]. The microwave power was adjusted such that the length of a  $\pi/2$  pulse was 15 ns corresponding to a microwave  $B_1$  field of 0.6 mT. The current transients after the pulse sequence are amplified, filtered, and recorded with a fast digitizer card. The relaxation times of the  $^{31}\text{P}$  and  $P_{b0}$  spins at the Si/SiO<sub>2</sub> interface are of the order of  $\mu\text{s}$  so that the experiment can be repeated with a repetition time of 800  $\mu\text{s}$  allowing the spin system to relax to its steady state [17]. The recorded current transients are boxcar integrated, giving an integrated charge  $\Delta Q$  which is directly proportional to the recombination rate at the end of the

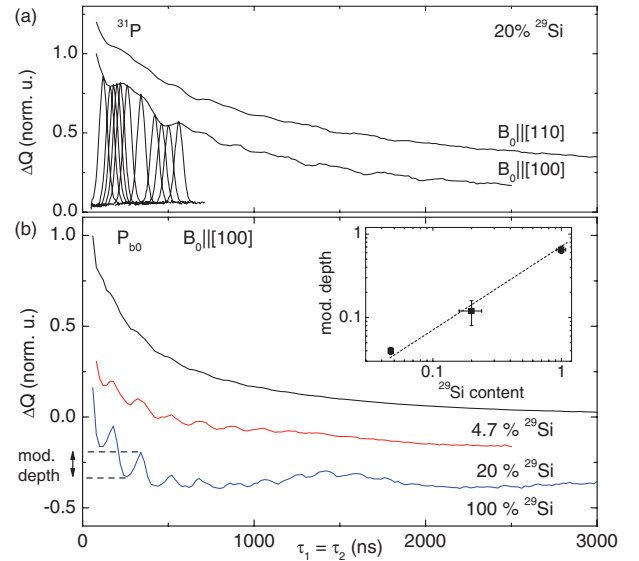


FIG. 2 (color online). (a) ESEEM signals (black lines) on the  $^{31}\text{P}$  resonance for  $\vec{B}_0 \parallel [100]$  and  $\vec{B}_0 \parallel [110]$  in the 20%  $^{29}\text{Si}$  sample. (b) ESEEM signals on the  $P_{b0}$  resonance for three samples with different  $^{29}\text{Si}$  concentrations for  $\vec{B}_0 \parallel [100]$ . The inset shows the modulation depths as a ( $\approx$  linear) function of the  $^{29}\text{Si}$  concentration for the main oscillation frequency.

microwave pulse sequence [18]. The signal-to-noise ratio is further improved by applying a lock-in technique switching the phase of the last  $\pi/2$  pulse [19].

To illustrate the EDESEEM technique and to demonstrate that the results are consistent with conventionally detected ESEEM, we measured EDESEEM traces on the high-field hf  $^{31}\text{P}$  resonance in the 20%  $^{29}\text{Si}$  sample. In Fig. 2(a),  $\Delta Q$  is shown as a function of the period of free evolution  $\tau_1 = \tau_2$  for two orientations of the sample with respect to the magnetic field. The normalized amplitudes of the traces are offset and in both, oscillations on a stretched exponential decay are clearly visible. For comparison, several echo traces for which  $\tau_1$  is kept fixed and  $\tau_2$  is varied are shown for  $\vec{B}_0 \parallel [100]$ . The peaks of the echoes coincide with the  $\tau_1 = \tau_2$  trace demonstrating the consistency of the two measurement methods. The oscillations can be attributed to anisotropic shf interactions with  $^{29}\text{Si}$  nuclear spins at the 4 nearest neighbor lattice sites around the  $^{31}\text{P}$  donor (so-called *E* shell) [20]. The ESEEM effect is usually discussed in terms of the diagonal  $A = A_{zz}$  and off-diagonal  $B^2 = A_{zx}^2 + A_{zy}^2$  parts of the hf tensor  $\vec{A}$  given in a coordinate system with  $\vec{B}_0 \parallel \hat{z}$ . The hf field gives rise to two nuclear modulation frequencies  $\nu_{\alpha/\beta} = \sqrt{(\nu_1 \pm A/2)^2 + B^2/4}$  which deviate from the free nuclear Larmor frequency  $\nu_1$ , resulting in an oscillation pattern on the echo decay [10], whereby the oscillation amplitude is given by the modulation depth  $k = (\nu_1 B / \nu_\alpha \nu_\beta)^2$ . From a fit of the data, we obtain  $\nu_\alpha = 3.27$  MHz and  $\nu_\beta = 2.79$  MHz for  $\vec{B}_0 \parallel [100]$  (3.62 MHz and 2.40 MHz for  $\vec{B}_0 \parallel [110]$ ), which agree well with the hf parameters reported in the literature [20,21].

Figure 2(b) shows the normalized ESEEM signals for the three samples with different  $^{29}\text{Si}$  concentrations for  $\vec{B}_0 \parallel [100]$  taken at the spectral positions ESEEM  $P_{b_0}$  indicated by arrows in Fig. 1. Although there is a spectral overlap between the peaks of the  $P_{b_1}$  and  $P_{b_0}$  centers, the factor of 4 smaller peak amplitude and the fact that for the  $P_{b_1}$  the mw pulses are off resonant allows us to assign the observed ESEEM signal to the  $P_{b_0}$  spins. In all three traces, oscillations with two main frequency components,  $\nu_1 \approx 5.7$  MHz and  $\nu_2 \approx 0.7$  MHz, on a stretched exponential background are visible becoming more pronounced for the samples with larger  $^{29}\text{Si}$  content. The modulation depth, taken as the amplitude of the faster oscillations after subtraction of the exponential background, scales approximately linearly with the  $^{29}\text{Si}$  content [inset of Fig. 2(b)]. Hence, we can conclude that the ESEEM signal originates from shf interactions of the  $P_{b_0}$  electron spin with surrounding  $^{29}\text{Si}$  nuclear spins.

Since  $\nu_1$  is about twice the nuclear frequency  $\nu_1$ , in principle, a simple one-to-one correspondence of the observed modulation frequencies  $\nu_1 = \nu_\alpha$  and  $\nu_2 = \nu_\beta$  can be assumed. The hf parameters are then given by  $\nu_\alpha \approx 2\nu_1 = A$  and  $\nu_\beta \approx B/2$  with the modulation depth  $k \approx (\frac{B\nu_1}{(B/2) \cdot 2\nu_1})^2$  close to unity, compatible with the observed results for the 100% sample. Within this simple scenario, the observed ESEEM signal can, thus, be attributed to  $^{29}\text{Si}$  nuclei with  $A \approx 5.7$  MHz and  $B \approx 1.2$  MHz. However, the assumption of only one type of nucleus contributing to the ESEEM signal cannot reproduce the slow beating of the oscillation maxima as seen in the 100%  $^{29}\text{Si}$  trace in Fig. 2(b). We, thus, have to consider several nuclei contributing to the modulation pattern, each with slightly different hf parameters. This scenario seems quite natural given that the basic [111] symmetry of Si/SiO<sub>2</sub> interface defects is lifted at the (100) silicon surface. However, to relate the observed shf parameters to the defect structure theoretical modeling is necessary.

We calculate the hf splittings as well as the electronic  $g$  tensor from first principles using a gauge-including projector augmented plane wave (GI-PAW) approach [22] as implemented in the QUANTUM-ESPRESSO package [23]. In the framework of density functional theory (DFT) we use the gradient-corrected Perdew-Burke-Ernzerhof functional in its spin-polarized form [24]. Since the hf splittings are determined by the magnetization density  $m(\vec{r})$  in a small region close to the nuclei they are calculated in scalar-relativistic approximation [25]. Supercells and periodic boundary conditions are used to model the structure of the  $P_{b_0}$  interface. Accordingly, the external magnetic field  $\vec{B}_0$  in the  $g$ -tensor calculation is described gauge invariantly [22,26]. Eight layers of crystalline Si atoms are simulated in a supercell giving rise to a total of 250 atoms. To ensure a well-defined transition to bulk material, the atoms in the lowest Si layer were saturated with H atoms and kept on their ideal bulk positions. All other atoms were allowed to relax freely. Since nonvanishing

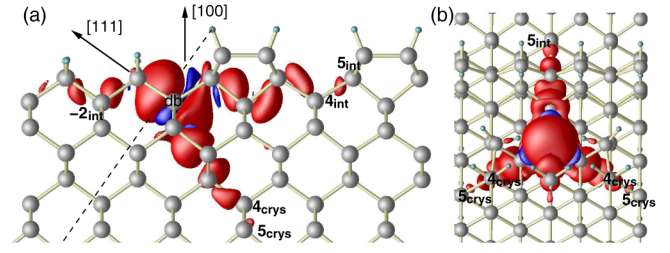


FIG. 3 (color online). Magnetization density  $m(\vec{r})$  of the most likely microscopic structure of the  $P_{b_0}$  center at the Si/SiO<sub>2</sub> (100) interface as determined from the comparison of ESEEM (100%  $^{29}\text{Si}$  sample) and theory: monolayer step with a dimerized upper part. View along  $[01\bar{1}]$  (a) and  $[111]$  (b). The lattice sites of nuclei contributing to the ESEEM signal are indicated.

values for  $m(\vec{r})$  are only found within a tripod formed by the three nearly equivalent zigzag lines into the crystalline part of the structure (cf. Fig. 3 and Ref. [26]), we expect almost vanishing hf interactions due to the  $^{29}\text{Si}$  nuclei in the oxide, in other words similar ESR parameters for a real Si/SiO<sub>2</sub> interface and a hydrogenated Si(100):H surface with the same coordination of the surface atoms.

We calculated the shf parameters for five different db-like model structures: for a flat H-terminated (100) surface without dimerization and for the same surface including a step either one or two monolayers high, both with and without dimerization, where the db is placed at the bottom of the step. In all cases the principal axis of the  $g$  tensor is [111] and the elements of the  $g$  tensor remain unchanged within  $\pm 0.0003$ . Similarly small variations ( $< 5\%$ ) are obtained for the hf splitting for  $\vec{B}_0 \parallel [100]$  at the db silicon atom itself ( $\approx 300$  MHz in good agreement with Ref. [4]) as well as for the second nearest neighbor ( $\approx 30$  MHz). Considerable differences, however, are found for some nuclei in the fourth and fifth layer below the db atom and an additional atom at the surface (lattice sites indicated in Fig. 3). Since these rather small hf splittings are strongly anisotropic, a dominant influence on the ESEEM spectrum can be expected. And indeed, if we fit the experimental data for the 100%  $^{29}\text{Si}$  sample using a model with seven nuclei and five different values of A and B (cf. Table I)

TABLE I. ESEEM parameters (in MHz for  $B_0 \parallel [100]$ ) of the hydrogenated 100%  $^{29}\text{Si}$  sample from a free fit to a model with 3 and 7 nuclear spins. For a coverage with native oxide (4.7%, 20%  $^{29}\text{Si}$  samples) similar values within 0.3 MHz (4th and 5th layer) and 0.9 MHz for  $-2_{\text{int}}$  are obtained (7-nuclei-fit). Also given are the corresponding theoretical values calculated from first principles for a  $P_{b_0}$ -like defect at a monolayer step including dimerization ( $b_0$ ) and for a flat surface ( $a$ ).

Site	# of sites	3-nuclei-fit		7-nuclei-fit		Theory $b_0$		Theory $a$	
		A	B	A	B	A	B	A	B
$4_{\text{crys}}$	2	5.3	1.2	5.4	1.2	5.5	1.1	5.8	1.1
$4_{\text{int}}$	1	6.5	1.3	6.5	1.1	6.4	1.0	7.0	1.4
$5_{\text{crys}}$	2			4.2	0.7	3.8	0.7	3.7	0.7
$5_{\text{int}}$	1			5.9	1.4	6.4	0.8	4.2	0.6
$-2_{\text{int}}$	1			7.7	1.4	7.6	1.4	9.8	2.0

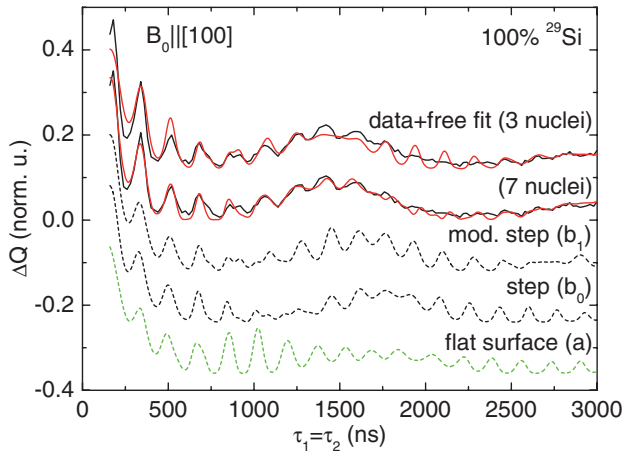


FIG. 4 (color online). ESEEM signal of the 100%  $^{29}\text{Si}$  sample (black solid line) with fits (red lines) taking into account three and seven nuclear spins. The corresponding fitting parameters are listed in Table I. Calculated ESEEM signals of the  $P_{b_0}$  at a dimerized monolayer-step structure ( $b_1$ ) and on a flat surface (a).

[27], the experimental ESEEM spectrum including the beating is reproduced very well (“data + free fit” in Fig. 4). For comparison, a fit with the three 4th layer nuclei only is shown as well, demonstrating that these nuclei are sufficient to reproduce at least the main features of the observed ESEEM signal.

Among the ESEEM spectra derived from *ab initio* calculations, the dangling bonds localized at steplike structures show the best agreement with the experimentally observed spectrum. Such steps are indeed likely to be present in the studied samples due to the slight off-axis cut. A further improvement is achieved if a dimerization of the last crystalline Si layer [7] at the upper part of the step is assumed. As an example, trace  $b_0$  in Fig. 4 shows the expected ESEEM signal using the calculated shf parameters (Table I) for the monolayer-step-like  $P_{b_0}$  structure with dimerization (Fig. 3). The basic modulation frequencies  $\nu_1$  and  $\nu_2$  as well as the beating observed in the experimental data are reproduced, only the frequency of the beating is too small. To illustrate which of the nuclei might be responsible for this deviation we adjusted the shf parameters of the 4th nearest neighbors by  $\approx 5\%$  to the experimental values. This places the maximum of the beating pattern at  $\tau_1 = 1500$  ns as observed in the experiment (trace  $b_1$ ). The destructive interference in the experimental data for  $\tau_1 > 1500$  ns could be caused by shf interactions with other nuclei not taken into account. For comparison, the ESEEM signal for a structure with a flat unreconstructed surface is shown in trace a in Fig. 4, but fails to reproduce basic experimental features like the characteristic beating pattern, thus demonstrating the sensitivity of the ESEEM signal with respect to the local defect structure.

The proof-of-concept study presented here suggests a more detailed interface investigation as a function of surface orientation, off-cut and termination (hydrogenated, thermal oxide). In particular, sample preparation by UHV techniques and UHV-ESR [28,29] will be beneficial.

The results in Fig. 2(b) already indicate a slight, but measurable difference in the shf properties of the  $P_{b_0}$  at HF-treated and oxide-terminated surfaces. The use of high- $k$  oxides would allow us to study the influence of the dielectric constant on the defect wave function. Advanced ESEEM pulse sequences [10] should increase the signal-to-noise ratio which in combination with measurements of the anisotropy of the ESEEM signal would allow a more detailed comparison with theory. In summary, taking the  $P_{b_0}$  defect at the Si/SiO<sub>2</sub> (100) interface as an example we have shown that EDESEEM in combination with *ab initio* calculations of the hf parameters is a powerful tool to study the microscopic structure of complex interfaces.

The work was funded by DFG (Grant No. SFB 631, C3, and SCHM 13621/11) and by BMBF (EPR-Solar).

*Note added in proof.*—EDESEEM can also be useful to study defects in device structures, e.g., solar cells [30].

\*hoehne@wsi.tum.de

- [1] J. Dąbrowski and H.-J. Müssig, *Silicon Surfaces and Formation of Interfaces* (World Scientific, Singapore, 2000).
- [2] E. H. Poindexter *et al.*, *J. Appl. Phys.* **52**, 879 (1981).
- [3] K. L. Brower, *Appl. Phys. Lett.* **43**, 1111 (1983).
- [4] W. E. Carlos, *Appl. Phys. Lett.* **50**, 1450 (1987).
- [5] J. L. Cantin *et al.*, *Phys. Rev. B* **52**, R11599 (1995).
- [6] A. Stesmans, B. Nouwen, and V. V. Afanas’ev, *Phys. Rev. B* **58**, 15 801 (1998).
- [7] A. Stirling *et al.*, *Phys. Rev. Lett.* **85**, 2773 (2000).
- [8] M. Cook and C. T. White, *Phys. Rev. B* **38**, 9674 (1988).
- [9] A. H. Edwards, *Phys. Rev. B* **36**, 9638 (1987).
- [10] A. Schweiger and G. Jeschke, *Principles of Pulse Electron Paramagnetic Resonance* (Oxford Univ. Press, New York, 2001).
- [11] D. R. McCamey *et al.*, *Appl. Phys. Lett.* **89**, 182115 (2006).
- [12] F. Hoehne *et al.*, *Phys. Rev. Lett.* **104**, 046402 (2010).
- [13] E. Abe *et al.*, *Phys. Rev. B* **82**, 121201 (2010).
- [14] A. Stesmans and V. V. Afanas’ev, *J. Phys. Condens. Matter* **10**, L19 (1998).
- [15] T. D. Mishima, P. M. Lenahan, and W. Weber, *Appl. Phys. Lett.* **76**, 3771 (2000).
- [16] C. F. Young *et al.*, *Phys. Rev. B* **55**, 16245 (1997).
- [17] H. Huebl *et al.*, *Phys. Rev. Lett.* **100**, 177602 (2008).
- [18] C. Boehme and K. Lips, *Phys. Rev. B* **68**, 245105 (2003).
- [19] F. Hoehne *et al.*, *Phys. Rev. Lett.* **106**, 187601 (2011).
- [20] E. B. Hale and R. L. Mieher, *Phys. Rev.* **184**, 739 (1969).
- [21] A. Ferretti *et al.*, *Phys. Rev. B* **72**, 235201 (2005).
- [22] C. J. Pickard and F. Mauri, *Phys. Rev. Lett.* **88**, 086403 (2002).
- [23] P. Giannozzi, *J. Phys. Condens. Matter* **21**, 395502 (2009).
- [24] J. P. Perdew, K. Burke, and M. Ernzerhof, *Phys. Rev. Lett.* **78**, 1396 (1997).
- [25] P. E. Blöchl, *Phys. Rev. B* **62**, 6158 (2000).
- [26] U. Gerstmann *et al.*, *Phys. Status Solidi (c)* **7**, 157 (2010).
- [27] Further free parameters are the amplitude, time constant, and exponent of the stretched exponential decay.
- [28] T. Umeda *et al.*, *Phys. Rev. Lett.* **86**, 1054 (2001).
- [29] M. Sterrer *et al.*, *Phys. Rev. Lett.* **94**, 186101 (2005).
- [30] M. Fehr *et al.* (to be published).